

Chapter 5

EVIDENCE FOR POLAR SHORT RANGE ORDER IN A NEMATOGEN

5.1 Introduction

In this chapter we report various experimental results on the compound p-cyanophenyl p-n heptylbenzoate (**CP7B**) which has an ester group in addition to a cyano end group which enhances considerably the dipole moment of the molecule. This leads to a large dielectric anisotropy ($\epsilon_a = 20$ at 35°C). The chemical structure and the transition temperatures of the compound are shown in Figure 5.1. The nematic phase easily supercools to room temperature making

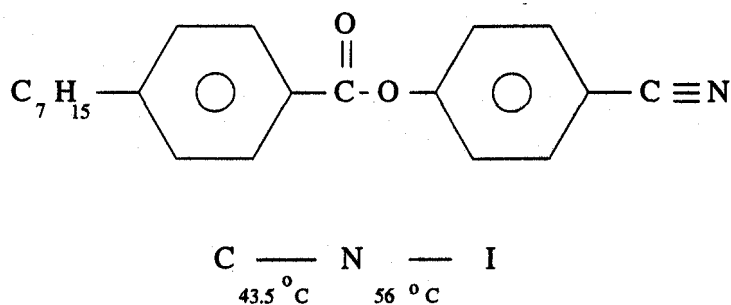


Figure 5.1: Chemical structure and transition temperatures of **CP7B**.

measurements over a large temperature range possible. The experimental studies indicate the presence of **polar short range order** in the medium. The results which will be discussed are:

- Electric field phase diagram of the **paranematic-nematic** phase transition.
- Field induced enhancement of the orientational order parameter in the nematic phase.
- Conductivity (σ_{\parallel}) measurements in the nematic phase and in particular the enhancement of σ_{\parallel} close to the field induced nematic-paranematic critical **point**.
- Divergence of the order parameter susceptibility near the electric field induced nematic-paranematic critical point using the third harmonic component of the electrical signal.
- Generation of a second harmonic response in the electrical signal near the **paranematic-nematic** critical point, which implies the presence of polar domains which do not reorient with the field.

- Evidence for a possible field induced phase transition.

The theoretical background on the effect of a strong electric field on the nematic-isotropic phase transition has been discussed in Chapters 2 and 3. We discuss the theoretical background for some of the other experimental studies in the next section. The experimental results and discussions are presented in Section 5.4.

5.2 Theoretical Background

5.2.1 Order Parameter Susceptibility : generation of the third harmonic component of the electric signal

Susceptibility is a measure of the response of a physical property to a conjugate field. In paramagnetic systems the magnetic field (H) is conjugate to the magnetisation (M), and the susceptibility (χ_H) is given by

$$\chi_H = \frac{\partial M}{\partial H}. \quad (5.1)$$

The order parameter S in the nematic phase, is conjugate to the square of the applied field i.e. E^2 (see Chapter 2). Hence one can define a susceptibility of the orientational order parameter S with respect to E^2 as

$$\chi_E = \frac{\partial S}{\partial E^2}. \quad (5.2)$$

As explained in Section 3.3.1.1, the relationship between ϵ_{\parallel} and the orientational order parameter S can be assumed to be of the form

$$\epsilon_{\parallel} = \bar{\epsilon} + \frac{2}{3}\Delta\epsilon_o S. \quad (5.3)$$

In the presence of an electric field the order parameter $S(E)$ is given by

$$S(E) = S(0) + \delta S(E) \quad (5.4)$$

where $S(0)$ is the field free order parameter and $\delta S(E)$ is the enhancement of the order parameter due to the field. From Equation 5.2 it can be seen that $\delta S(E)$ is proportional to E^2 (ignoring the linear dependence on the **magnitude** of E due to the quenching of thermal fluctuations of the director, which will be discussed in the next section)

$$\delta S(E) = \chi_E E^2. \quad (5.5)$$

In our experiments we conduct an electrical impedance analysis of the sample cell. To relate χ_E with the measured signal we calculate the current flowing through the cell taking into account the quadratic dependence of δS on E .

The capacitance of the sample is given by

$$C_s = C_o \epsilon_{\parallel} \quad (5.6)$$

where C_o is the capacitance of the empty cell.

$$\begin{aligned} C_s &= C_o \left(\bar{\epsilon} + \frac{2}{3}\Delta\epsilon_o S \right) \\ &= C_a + C_2 E^2 \end{aligned} \quad (5.7)$$

where

$$C_a = C_o \left(\bar{\epsilon} + \frac{2}{3} \Delta\epsilon_o S(0) \right)$$

and

$$C'_2 = C_o \left(\frac{2}{3} \Delta\epsilon_o \chi E \right). \quad (5.8)$$

If the voltage applied to the sample cell is $V = V_o \sin \omega t$ where $\omega = 2\pi f$ and f is the frequency of the applied voltage, the field is $E \sin \omega t = V_o \sin \omega t / d$, where d is the thickness of the cell. Considering only a capacitive response of the sample cell the current flowing through it is given by

$$\begin{aligned} I &= \frac{d}{dt}(C_s V) \\ &= \frac{d}{dt} \{ [C_a + C_2 V_o^2 \sin^2 \omega t] [V_o \sin \omega t] \} \\ &= V_o \omega \cos \omega t (C_a + C_2 V_o^2 \sin^2 \omega t) + V_o \sin \omega t [2\omega C_2 V_o^2 \sin \omega t \cos \omega t] \\ &= V_o \omega [C_a \cos \omega t + 3C_2 V_o^2 \sin^2 \omega t \cos \omega t] \\ &= V_o \omega \left\{ C_a + \frac{3}{4} V_o^2 C_2 \right\} \cos \omega t - \frac{3}{4} V_o^2 C_2 \cos 3\omega t \end{aligned} \quad (5.9)$$

where $C_2 = C'_2 / d^2$, and $\sin^2 \omega t \cos \omega t = \frac{1}{4} [\cos \omega t - \cos 3\omega t]$.

Thus a quadratic dependence on the electric field of the enhancement of the order parameter leads to the generation of a third harmonic component in the current passing through the sample. As we are measuring the voltage drop across a series capacitor C_m the third harmonic component of the measured voltage is given by

$$V_3 = \frac{3 V_o^3 C_2}{8 C_m} \quad (5.10)$$

From Equation 5.8 it is seen that

$$\begin{aligned} \chi E &= \frac{3 C'_2}{2 C_o \Delta\epsilon_o} \\ &= \left(\frac{4 C_m d^2}{C_o \Delta\epsilon_o V_o^3} \right) V_3. \end{aligned} \quad (5.11)$$

Hence the third harmonic component of the electrical signal is a measure of the electric susceptibility of the order parameter. It can be seen from the above derivation that to generate a second harmonic response the enhancement of the order parameter should depend linearly on the applied field. This is possible only if there are polarised domains which do not reorient with the applied electric field.

Near a critical point the susceptibility diverges following a power law [73]. According to the Landau theory (see Equation 3.13 of Section 3.2.3) the equilibrium condition for S in the presence of E is given by

$$a(T - T^*)S - BS^2 + CS^3 - \frac{1}{12\pi} \Delta\epsilon_o E^2 = 0. \quad (5.12)$$

We are interested in calculating the variation of the order parameter susceptibility near the electric field induced nematic-paranematic critical point. Differentiating Equation 5.12 with

respect to E^2 we find that

$$\chi_E = \frac{\partial S}{\partial E^2} = \frac{\frac{1}{12\pi} \Delta \epsilon_o}{a(T - T^*) - BS + CS^2}. \quad (5.13)$$

At the critical point $S = S_c$. Expressing T^* and S_c in terms of the Landau coefficients and T_c (Equation 3.14) we get

$$\chi_E = \frac{\Delta \epsilon_o}{12\pi a(T - T_c)}. \quad (5.14)$$

Hence according to the Landau theory the order parameter susceptibility near the critical point shows a power law divergence

$$\chi_E \propto (T - T_c)^{-1}. \quad (5.15)$$

In Sections 5.4.4 and 5.4.5 we present measurements of the third harmonic component of the electrical signal in the vicinity of the nematic-paranematic electric field critical point.

5.2.2 Electric Field Quenching of Thermal Fluctuations of the Director

In the previous section we used the dielectric interaction of the director with an applied electric field, leading to a quadratic dependence of the enhancement of S on E . This arises from the second rank tensor nature of the physical properties of the nematic liquid crystalline medium. This effect has a microscopic origin and is usually known as the Kerr effect. As mentioned in Chapter 2, the macroscopic thermal fluctuations of the director are also suppressed under the action of a magnetic field (or equally an electric field), thus leading to an enhancement of the order parameter [1, 22]. This increase in order parameter is both linearly and quadratically dependent on the magnitude of the applied electric field.

To discuss the effect of a field on the thermal fluctuations in a nematic medium, we follow the derivation given by de Gennes [1]. Consider a nematic sample with its optical axis along \hat{z} . The average director A is parallel to \hat{z} . The thermal fluctuations of the optical axis at any point \vec{r} can be described by the small nonzero components $n_x(\vec{r})$ and $n_y(\vec{r})$. The elastic distortion energy for a nematic liquid crystal is given by

$$F_d = \int \left\{ \frac{1}{2} K_1 (\nabla \cdot \hat{n})^2 + \frac{1}{2} K_2 (\hat{n} \cdot \nabla \times \hat{n})^2 + \frac{1}{2} K_3 (\hat{n} \times \nabla \times \hat{n})^2 \right\} d\vec{r} \quad (5.16)$$

where K_1 , K_2 , K_3 are the splay, twist, and bend elastic constants as described in Chapter 1.

In terms of n_x and n_y the distortion energy (Equation 5.16) reduces to

$$F_d = \int \left\{ \frac{1}{2} K_1 \left(\frac{\partial n_x}{\partial x} + \frac{\partial n_y}{\partial y} \right)^2 + \frac{1}{2} K_2 \left(\frac{\partial n_x}{\partial y} - \frac{\partial n_y}{\partial x} \right)^2 + \frac{1}{2} K_3 \left[\left(\frac{\partial n_x}{\partial z} \right)^2 + \left(\frac{\partial n_y}{\partial z} \right)^2 \right] \right\} d\vec{r}. \quad (5.17)$$

As explained in Chapter 2, in the presence of an electric field we add a term to the free energy which couples the director with the electric field through the dielectric anisotropy.

$$F^E = -\frac{1}{8\pi} \int \epsilon_a E^2 (n_x^2 + n_y^2) d\vec{r} + C \quad (5.18)$$

where C is a constant. It is convenient to analyse $n_x(\vec{r})$, and $n_y(\vec{r})$ in Fourier components, defined by

$$n_x(\vec{q}) = \int n_x(\vec{r}) e^{i\vec{q} \cdot \vec{r}} d\vec{r}. \quad (5.19)$$

In terms of these Fourier components the free energy becomes

$$F = F_o + \frac{1}{2}\Omega^{-1} \sum_q \{K_1 |n_x(\vec{q})q_x + n_y(\vec{q})q_y|^2 + K_2 |n_x(\vec{q})q_y - n_y(\vec{q})q_x|^2 + (K_3 q_z^2 + \frac{\epsilon_a}{4\pi} E^2) \{|n_x(\vec{q})|^2 + |n_y(\vec{q})|^2\}\} \quad (5.20)$$

where Ω is the sample volume. For a given q it is convenient to diagonalise the quadratic form in Equation 5.20 by a linear transformation $(n_x, n_y) \rightarrow (n_1, n_2)$. The meaning of the axes (1) and (2) is the following. Introducing for each \vec{q} two unit vectors \hat{e}_1 and \hat{e}_2 in the (xy) plane \hat{e}_2 is normal to \vec{q} and \hat{e}_1 is normal to \hat{e}_2 . The component of $n(\vec{q})$ along 2 is called $n_2(q)$ ($a=1,2$). $n_1(\vec{q})$ describes a periodic distortion which is a mixture of splay and bend. $n_2(\vec{q})$ is a periodic distortion which is a mixture of twist and bend. In terms of n_1 and n_2 the free energy takes a simple form

$$F = F_o + \frac{1}{2}\Omega^{-1} \sum_q \sum_{\alpha=1,2} |n_\alpha(q)|^2 (K_3 q_{\parallel}^2 + K_\alpha q_{\perp}^2 + \frac{\epsilon_a}{4\pi} E^2) \quad (5.21)$$

where $q_{\parallel} = q_z$ is the component of the wave vector parallel to the optic axis while q_{\perp} is the normal component. Applying the equipartition theorem for a classical system the average energy for each fluctuation mode at thermal equilibrium is equal to $\frac{1}{2}k_B T$

$$\langle |n_\alpha|^2 \rangle = \frac{\Omega k_B T}{K_3 q_{\parallel}^2 + K_\alpha q_{\perp}^2 + \frac{\epsilon_a}{4\pi} E^2}. \quad (5.22)$$

where the brackets $\langle \rangle$ denote a thermal average. For simplicity making a one constant approximation and inverting the Fourier transform of Equation 5.22 we get

$$\langle n_x^2(\vec{r}) \rangle = (2\pi)^3 \int \frac{k_B T}{K(q^2 + \xi^{-2})} dq \quad (5.23)$$

where ξ is an electrical coherence length [1] defined by

$$\xi(E) = \left(\frac{K}{\frac{\epsilon_a}{4\pi}} \right)^{\frac{1}{2}} \frac{1}{|E|}. \quad (5.24)$$

Integrating over q with $q_{max} \sim 1/a$ (where a is of the order of a molecular dimension)

$$\langle n_x^2 \rangle = \frac{k_B T}{2\pi^2 K} (q_{max} - \frac{\pi}{2\xi}) = \langle n_y^2 \rangle. \quad (5.25)$$

$\langle n_z^2 \rangle = 1 - \langle n_x^2 \rangle - \langle n_y^2 \rangle$ and the effective anisotropy of the dielectric constant is

$$\langle \epsilon_{\parallel} - \epsilon_{\perp} \rangle = \Delta\epsilon_o \left(\frac{3}{2} \langle n_z^2 \rangle - \frac{1}{2} \right) \quad (5.26)$$

which can be written in the form

$$\begin{aligned} \langle \epsilon_{\parallel} - \epsilon_{\perp} \rangle &= \epsilon_a(T) + \frac{3\Delta\epsilon_o k_B T}{4\pi K \xi} \\ &= \epsilon_a(T) + \frac{3\Delta\epsilon_o k_B T}{4\pi K^{\frac{3}{2}}} \left(\frac{\epsilon_a}{4\pi} \right)^{\frac{1}{2}} |E|. \end{aligned} \quad (5.27)$$

As

$$S = \frac{\langle \epsilon_{\parallel} - \epsilon_{\perp} \rangle}{\Delta \epsilon_0} \quad (5.28)$$

it can be seen that the increase in the order parameter due to the quenching of the thermal fluctuations is given by

$$\Delta S = \frac{3k_B T}{4\pi K^{3/2}} \left(\frac{\epsilon_a}{4\pi} \right)^{\frac{1}{2}} |E| = c_l |E|. \quad (5.29)$$

This contribution to the enhancement in S is linear in $|E|$ and becomes quite important near the nematic-paranematic transition when K is small.

The quenching of the macroscopic thermal fluctuations with a stabilising field contributes to SS at higher orders in field [37] due to the dependence of ϵ_a and K on S . Using a Taylor expansion we can write

$$\delta S = \left(\frac{\partial S}{\partial E} \right) + \frac{1}{2} \left(\frac{\partial^2 S}{\partial E^2} \right). \quad (5.30)$$

As in principle $K \propto \frac{1}{S^2}$ and $\epsilon_a \propto S$,

$$\delta S(E) = c_l |E| - \frac{5}{2} \frac{c_l^2}{S(0)} E^2. \quad (5.31)$$

The increase in the order parameter due to the microscopic Kerr effect is given by :

$$\delta S_{qk} = \frac{\chi_k \epsilon_a}{12\pi} E^2 \quad (5.32)$$

where χ_k is an appropriate susceptibility.

Thus the total induced order $\delta S(E)$ from a stabilising electric field is

$$\begin{aligned} \delta S(E) &= c_l |E| + c_q |E^2| \\ &= c_l |E| + (c_{ql} + c_k) |E^2| \end{aligned} \quad (5.33)$$

where c_l is the linear coefficient in Equation 5.29 and c_q is a sum of the quadratic enhancement of the order parameter due to the microscopic Kerr effect (c_k) and the saturation effect due to the quenching of the thermal fluctuations (c_{qk}). In Section 5.4.3 we present measurements of the order parameter in a nematic liquid crystal as functions of temperature and field.

5.3 Experimental Procedure

For these experiments we used the improved experimental setup described in Chapter 2 (see Figure 2.20). We used a cell with the guard ring (Figure 2.3). The top counter electrode was an ITO coated conducting glass plate. We have measured the thickness of the cells using the interferometric technique as described in Chapter 2. Near the critical region it can be seen from Figure 3.11 in Chapter 3 that the variation of the order parameter is highly nonlinear with the electric field. To measure the nonlinear components of the electrical signal we have included in our programme the measurements of the second and third harmonic components using the lock-in-amplifier. The scattered intensity from the sample is simultaneously measured.

The temperature is reduced in preset steps with a constant sinusoidal voltage applied to the cell and the stability is monitored by the platinum resistance thermometer fixed near the sample. The field free resistance of the nickel resistance thermometer is measured before and after every voltage run at the extreme limits of the temperature range to check its stability.

INPUT
 TEMPERATURE -T
 VOLTAGE -V
 START TEMPERATURE -ST
 END TEMPERATURE -ET
 TEMPERATURE STEP -TS
 WAIT TIME -T1, T2
 START VOLTAGE -SV
 END VOLTAGE -VE
 VOLTAGE STEP -DV
 POST EXPERIMENT TEMPERATURE -PET
 RATIO OF OUT OF PHASE VOLTAGE TO IN PHASE VOLTAGE -VR

TEMPERATURE STABILITY -DTS
 ELECTRICAL SIGNAL -V_m
 NICKEL RESISTANCE - R
 TEMPERATURE STABILITY -DTS
 HARMONICS - H1, H2...HN
 DIODE OUTPUTS D1, D2

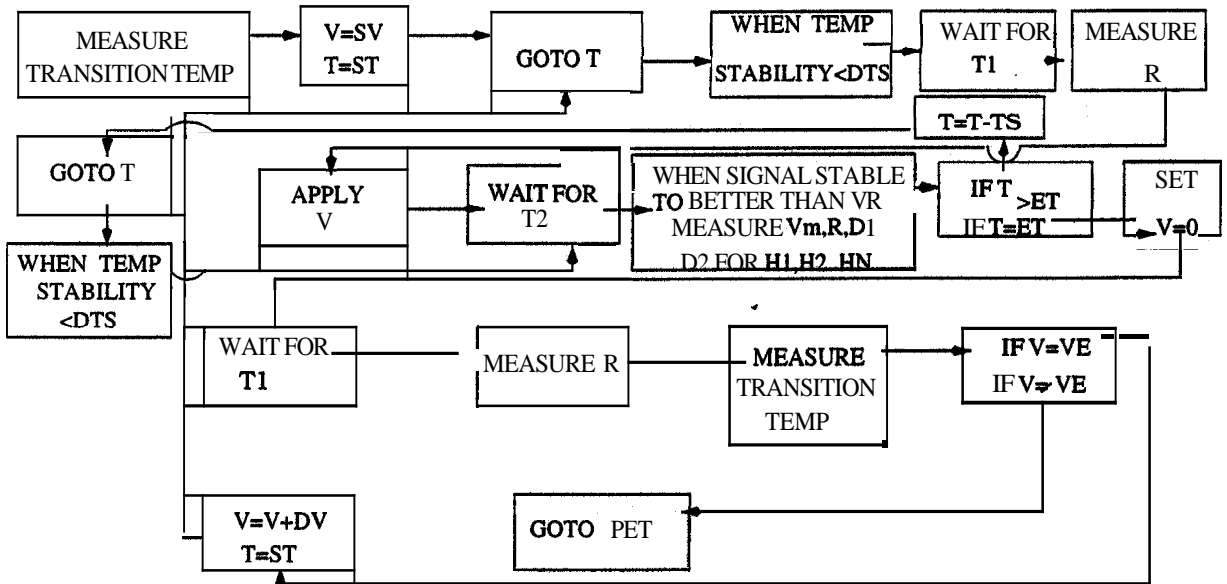


Figure 5.2: Flow chart for the programme used for conducting the experiments.

When a high voltage is constantly applied to the sample it slowly deteriorates thus leading to a shift in the transition temperature. The shift depends on the voltage applied and the sample used. For the sample **CP7B** the shift in the transition temperature varied from $< 0.1^{\circ}\text{C}$ for $V = 10\text{ V}$ and $\sim 0.5^{\circ}\text{C}$ for $V = 200\text{ V}$, for a $16\mu\text{m}$ sample, when the voltage is constantly applied for ~ 24 hours. To take into account this shift in the transition temperature we measure the field free transition temperature before and after each of the voltage runs. A linear interpolation is used to estimate the transition temperature at a given time. The flow chart for the programme of this experiment is shown in Figure 5.2.

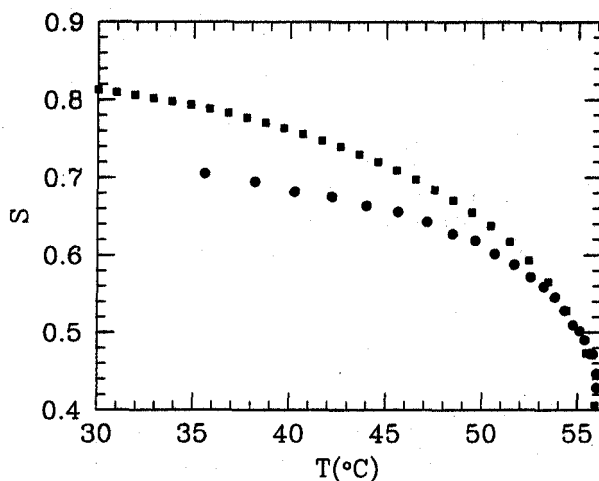


Figure 5.3: Comparison between the orientational order parameter measured from magnetic susceptibility (circles) and the dielectric constant (squares) ϵ_{\parallel} in the compound **CP7B**. The dielectric data has been normalised at $T - T_{NI} = 2^{\circ}\text{C}$, and the higher effective value S_e compared to the true value S indicates a change in the short range order of the medium at lower temperature.

5.4 Results and Discussion

5.4.1 Low Field Dielectric Measurements

The temperature dependence of the magnetic susceptibility of **CP7B** has been measured (which will be described in Chapter 7) and agrees to within $\sim 8\%$ with the values reported earlier by **Buka** and de Jeu [74]. Using this data we have calculated the absolute order parameter as a function of temperature (Figure 5.3). Using the impedance analysis of the cell filled with **CP7B** we have measured ϵ_{\parallel} . The sample thickness is $\simeq 16\ \mu\text{m}$ and the applied voltage is 10 V (~ 20 esu) which is sufficiently low so that the ϵ_{\parallel} data can be considered as 'zero field' values. Our dielectric measurement of ϵ_{\parallel} agrees to within 2% with the values reported earlier by Titov *et al* [75]. We can write as described in Chapter 1 [3]

$$\epsilon_{\parallel} \simeq \bar{\epsilon} + \left\{ \frac{2}{3} A \left(\Delta\alpha + \frac{F\mu^2}{k_B T} \right) \right\} S \quad (5.34)$$

where $\bar{\epsilon}$ is the average dielectric constant, A and F are correction factors for local field effects, $\Delta\alpha$ the anisotropy of polarisability and μ the dipole moment assumed to be parallel to the long axis of the molecule and k_B the Boltzmann constant.

The *main* contribution to the dielectric constant comes from the orientation polarisation arising from the 'effective' dipole moment μ of the molecule. Hence one would expect from Equation 5.34 that $(\epsilon_{\parallel} - \bar{\epsilon})$ is a measure of S/T . Normalising the order parameter near T_{NI} with respect to the magnetic susceptibility data, and taking out the above temperature dependence, we have calculated the 'order parameter' S_e as a function of temperature (Figure 5.3). It is clear that S_e has a substantially higher value at lower temperatures compared to the true order parameter S , indicating that the effective μ is also increasing at lower temperatures.

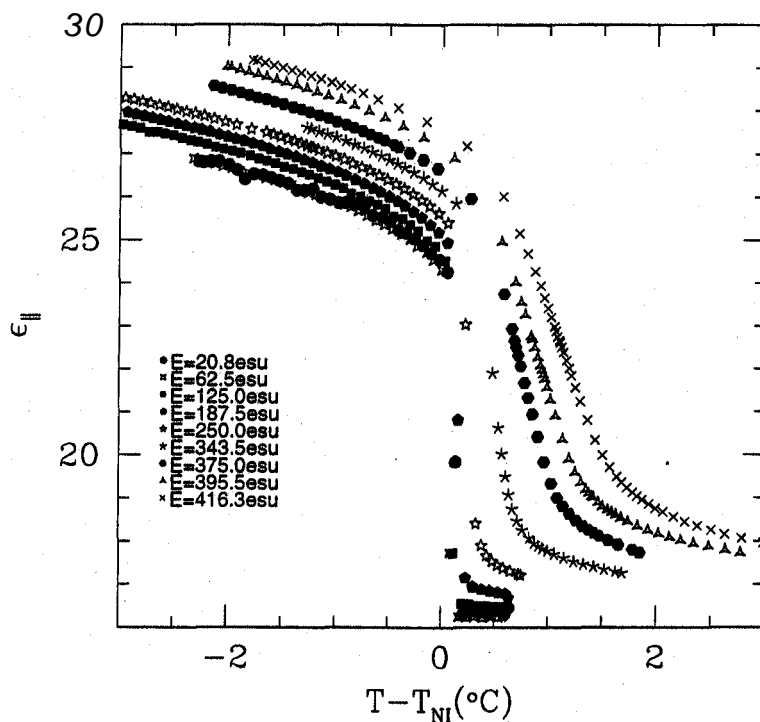


Figure 5.4: Variation of $\epsilon_{||}$ across the nematic-paranematic transition region as a function of $T - T_{NI}$ for different fields. $d=16$ pm, $f=4111$ Hz.

This is possible if the short range order changes with temperature. Indeed in the molecular theory of such highly polar compounds referred to in the previous chapter [58, 59], the relative concentration of *parallel* configuration which has a higher effective dipole moment must increase at lower temperatures. It is clear that in **CP7B** this mechanism appears to lead to the strong variation in $\epsilon_{||}$ in the temperature range of interest. On the other hand, in compounds like **5CB**, **7CB** etc., the order parameter calculated from the dielectric measurement is proportional to that obtained from the magnetic susceptibility measurement to a good approximation [76]. As such, a significant temperature variation of the relative concentration of parallel and antiparallel configurations can occur only far below the observed nematic range in the latter cases.

5.4.2 Electric Field Phase Diagram

We have measured $\epsilon_{||}$ of **CP7B** across the paranematic-nematic phase transition temperature for different fields as shown in Figure 5.4.

We have used the orientational order parameter obtained from magnetic susceptibility measurements (described in Chapter 7) at $T_{NI} - 2^\circ$ to evaluate $\Delta\epsilon_o$ ($=25.2$) (see Figure 5.3). It can be seen from Figure 5.3 that this calibration is valid close to the nematic-isotropic transition temperature. Figure 5.5 shows the variation of the order parameter at different fields calculated from the dielectric data as a function of temperatures close to the transition point. The thickness of the sample is $16\mu\text{m}$ and the frequency of the applied voltage is 4111 Hz. In the nematic range the curves are almost parallel. Also close to the critical field it is seen that the points become more scarce. This is due to a large local heating around the critical region (as will be discussed in Section 5.4.4). Also, as discussed in Chapter 3 the Landau theory is insufficient to

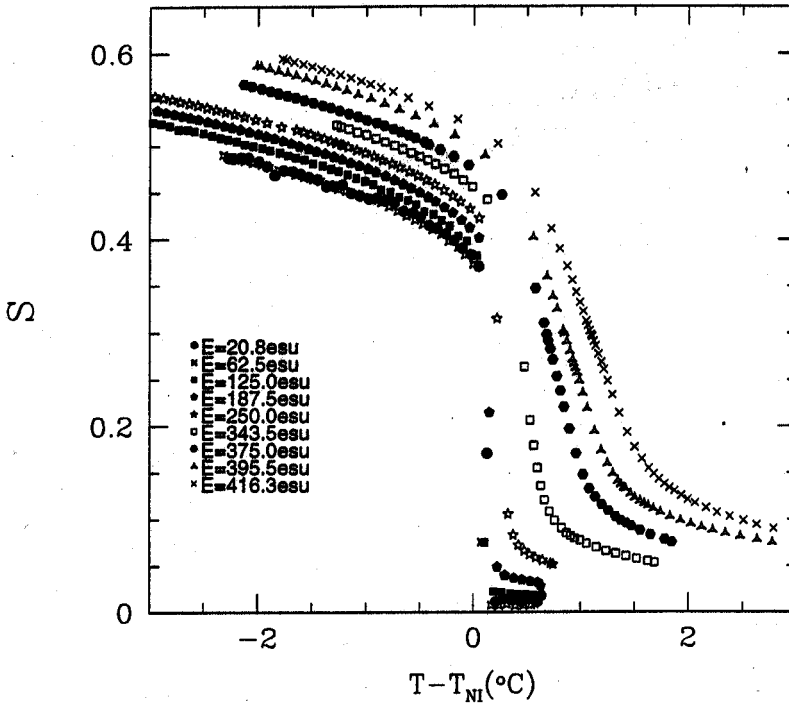


Figure 5.5: Variation of the order parameter as a function of $T - T_{NI}$, calculated from the data taken from Figure 5.4

describe the experimental curves. Taking all these points into consideration we have not tried to fit this data to the Landau model.

5.4.3 Field Enhanced Order Parameter Measurements

We have measured the variation of ϵ_{\parallel} in the nematic range for different applied fields. As shown in Section 5.4.1 it is not possible to obtain a 'correct' order parameter throughout the temperature range by **normalising** the data at one temperature. This calibration is valid only close to the nematic-isotropic transition. To obtain a one to one calibration curve for the order parameter from the magnetic susceptibility data (shown in Figure 5.3) we plot the ϵ_{\parallel} measured at $V = 10$ V as a function of S (Figure 5.6). From this **calibration curve** we calculate the **order parameter** for a given measured value of ϵ_{\parallel} .

Figure 5.7 shows the variation of ϵ_{\parallel} at different fields as a function of temperature over a wide temperature range in the nematic phase. It is interesting to note that the experimental curves remain roughly parallel to one another even when the temperature is $\sim 25^{\circ}$ below the transition point. One would have expected that as the order parameter susceptibility decreases rapidly at lower temperatures, the different curves would have crowded together. (The latter trend is in fact seen in the 8OCB-6OCB mixture shown in Figure 4.10).

Figure 5.8 shows the order parameter of CP7B calculated as explained above at different fields as a function of temperature. It is obvious that even the order parameter curves at different fields do not crowd together at lower temperatures. We have interpolated the data from Figure 5.8 and calculated $\delta S(E)$ at a few temperatures. We have fitted this $\delta S(E)$ data to an equation of the form $\delta S(E) = c_1 E + c_2 E^2$, where c_1 is the linear coefficient related to the enhancement

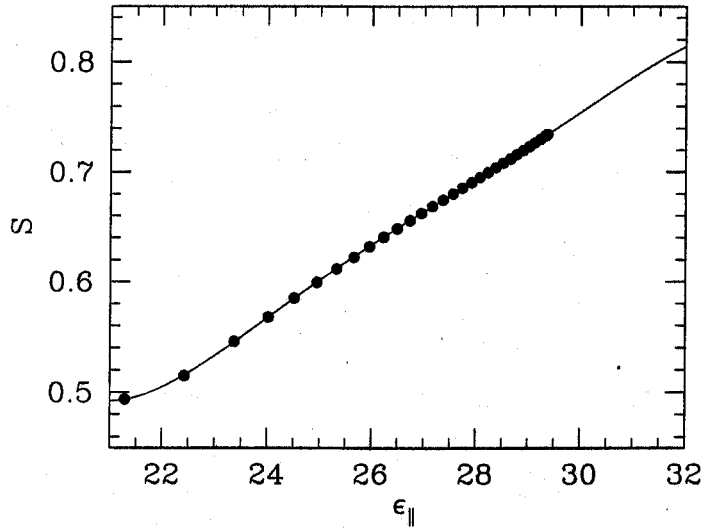


Figure 5.6: Calibration of ϵ_{\parallel} against the order parameter data as measured by the magnetic susceptibility. The fit corresponds to a fifth order polynomial $S = 121.36688497 - 22.697520672\epsilon_{\parallel} + 1.69170\epsilon_{\parallel}^2 - .062656722\epsilon_{\parallel}^3 + .0011550214\epsilon_{\parallel}^4 - 8.479429\epsilon_{\parallel}^5$

of the order parameter due the quenching of the thermal fluctuations and c_q is the quadratic coefficient, related both to the Kerr effect and the quenching of thermal fluctuations (as described in Section 5.2.2). Figure 5.9 shows $\delta S(E)$ as a function of field at a few temperatures in the nematic range. Figure 5.10 shows a plot of the linear and nonlinear coefficients as a function of temperature. It can be seen that as the temperature is decreased c_l decreases with temperature whereas c_q initially decreases and then starts to increase at $\sim 53^\circ\text{C}$.

To compare these results with the theoretical predictions described in Section 5.2.2 we calculate the expected contributions to the enhancement of the order parameter from the quenching of the thermal fluctuations and the Kerr effect. According to Equation 5.29

$$\Delta S(E) = \frac{3k_B T}{4\pi K^{3/2}} \left(\frac{\epsilon_a}{4\pi} \right)^{\frac{1}{2}} |E|$$

As mentioned in Section 5.2.2 it is expected that $\epsilon_a \propto S$ and $K \propto S^2$ and hence $c_l \propto S^{-2.5}$. However the actual variation of c_l with S is much less rapid. Malraison *et al* [77] experimentally measured the magnetic quenching of thermal fluctuations in 7CB and 80CB and used measured values of the susceptibility anisotropy (χ_a) and the elastic constants and found that the theoretical variation was considerably greater than the experimental variation near T_{NI} . Hence the deviation indicates that the mean field theory is not adequate enough to describe the experimental data. In our experiments we see that $c_l \propto S^{-0.96}$ (Figure 5.11) which is a much slower variation than the expected variation *viz.* $\propto S^{-2.5}$. Also as mentioned in Section 5.2.2 c_l depends on S and gives rise to a change in the order parameter quadratic in E . Using the empirically found relation of $c_l = \frac{\delta S}{\delta E} = \lambda S^{-0.96}$, we obtain $\frac{\delta^2 S}{\delta E^2} = c_{ql} \simeq -\frac{0.96\lambda^2}{S^{-2.88}}$ (Figure 5.12) which produces a saturation with field, as it has a negative sign. by taking out the quadratic contribution we can calculate the enhancement of S due to the Kerr effect.

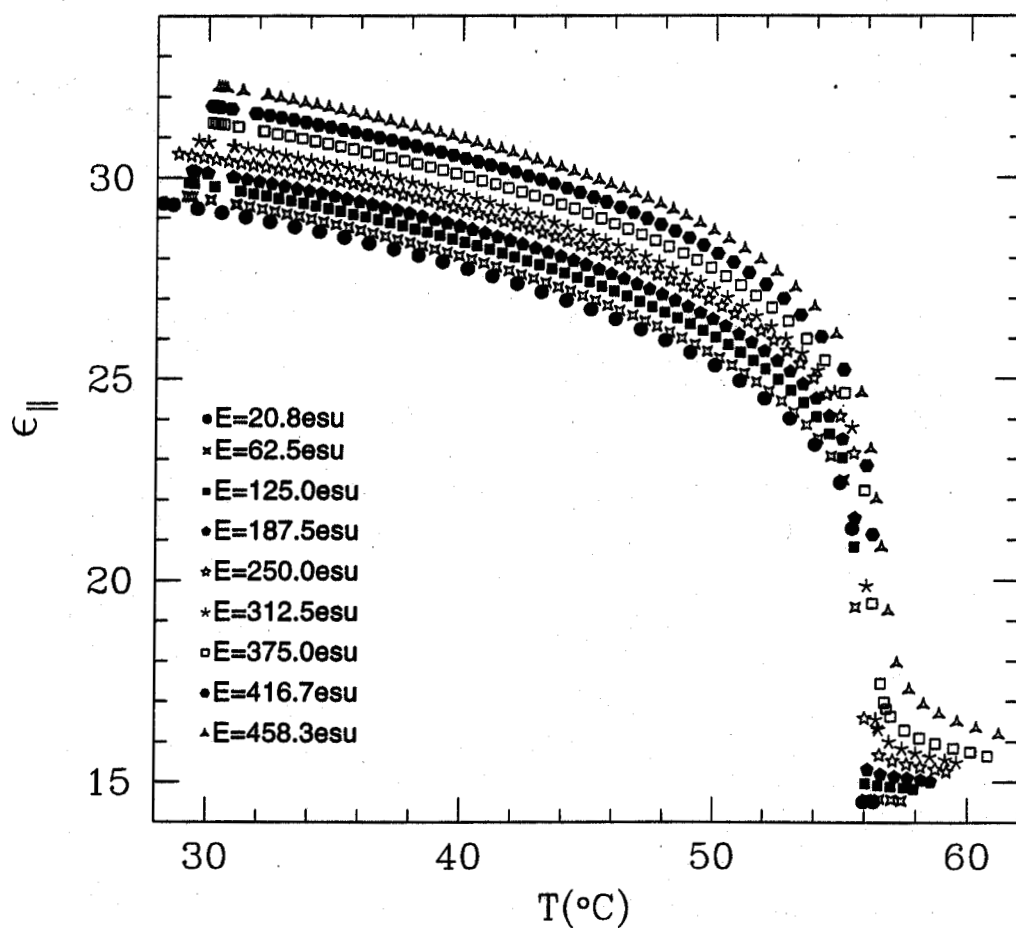


Figure 5.7: Variation of $\epsilon_{||}$ as a function of temperature in the nematic range of CP7B at different fields. $d = 16 \mu\text{m}$, $f = 4111$ Hz.

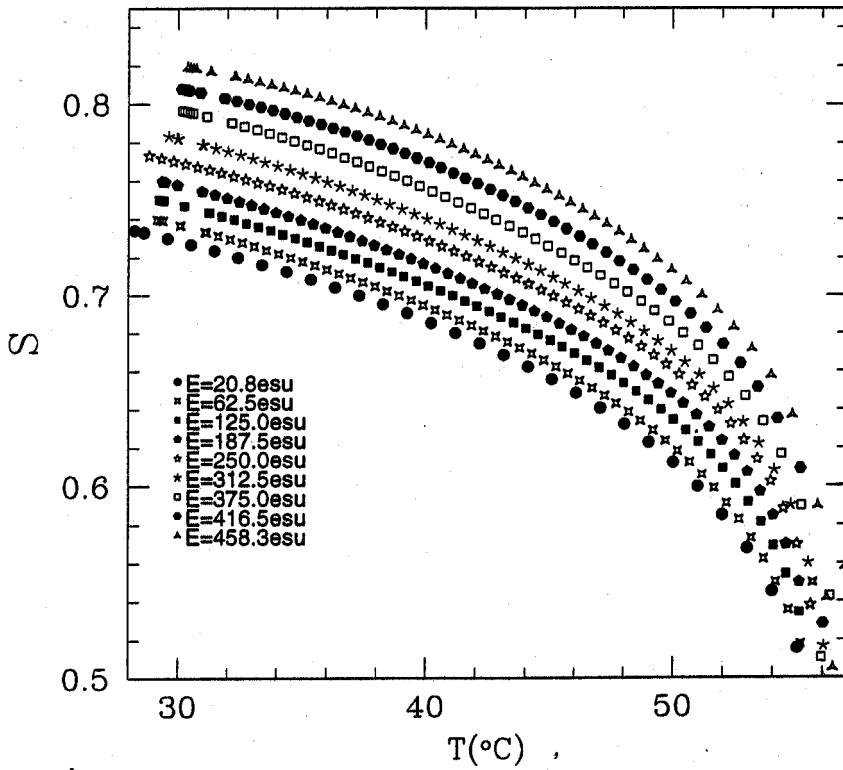


Figure 5.8: Variation of the order parameter calculated from the data shown in Figure 5.7

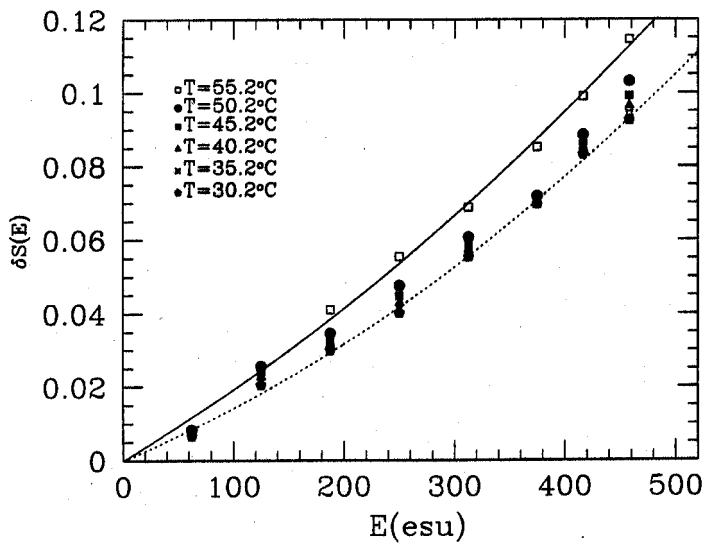


Figure 5.9: Variation of the $\delta S(E)$ as a function of the electric field at a few temperatures in the nematic range of CP7B. The lines are fits to the functional form $\delta S(E) = c_1 E + c_2 E^2$. For clarity we have shown only two of the fitted variations.

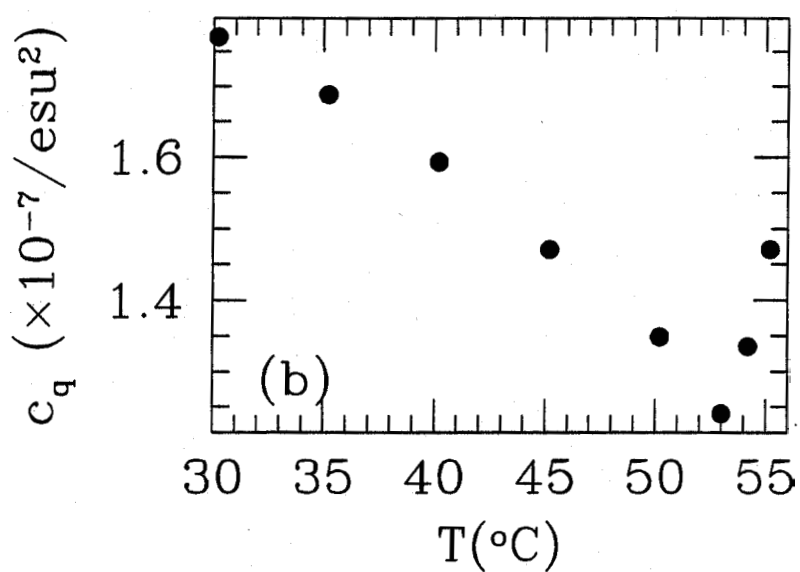
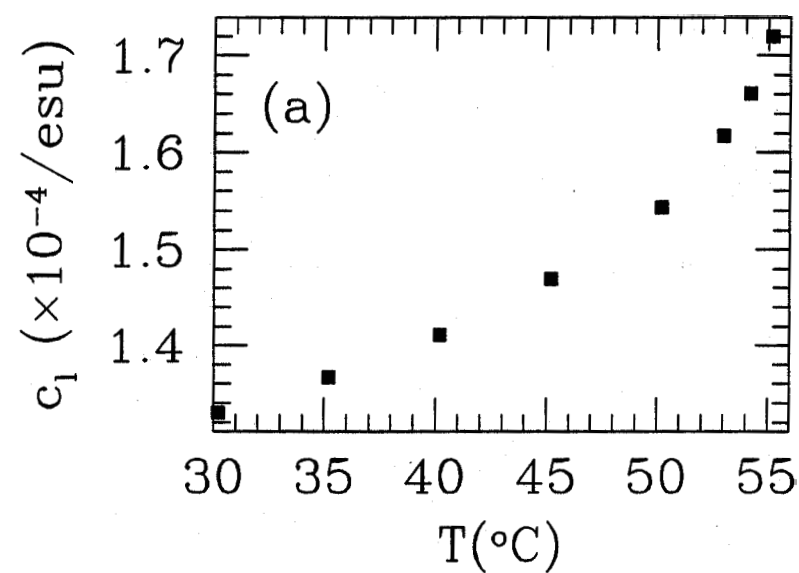


Figure 5.10: (a) Variation of the coefficient c_l as a function of temperature. (b) Variation of c_q as a function of temperature. Data taken from the fitted curves shown in Figure 5.9.

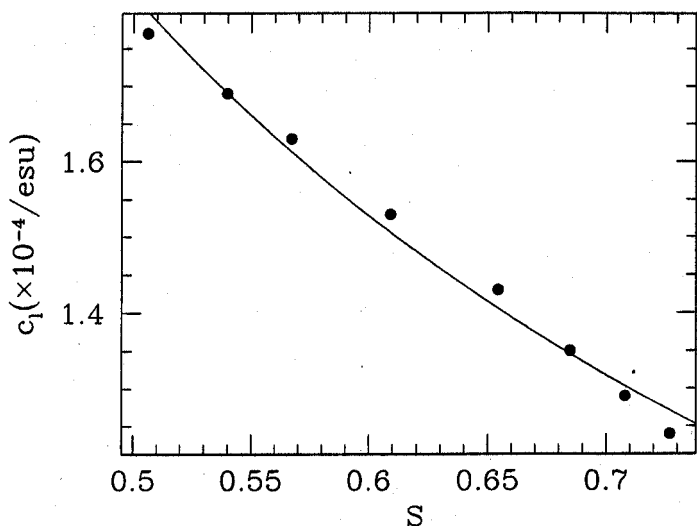


Figure 5.11: Variation of c_l as a function of $S(0)$ The line corresponds to the functional form $c_l = \lambda S^{-0.96}$ where $\lambda = 9.356 \times 10^{-5} / \text{esu}$.

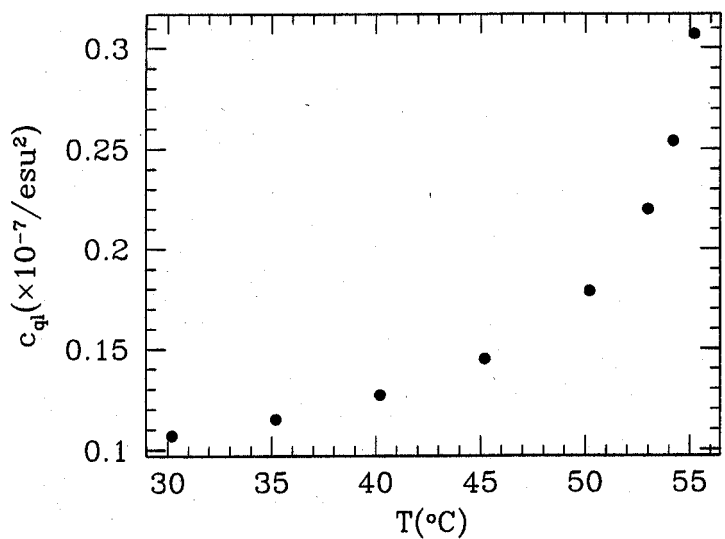


Figure 5.12: Variation of c_{ql} as a function of temperature.

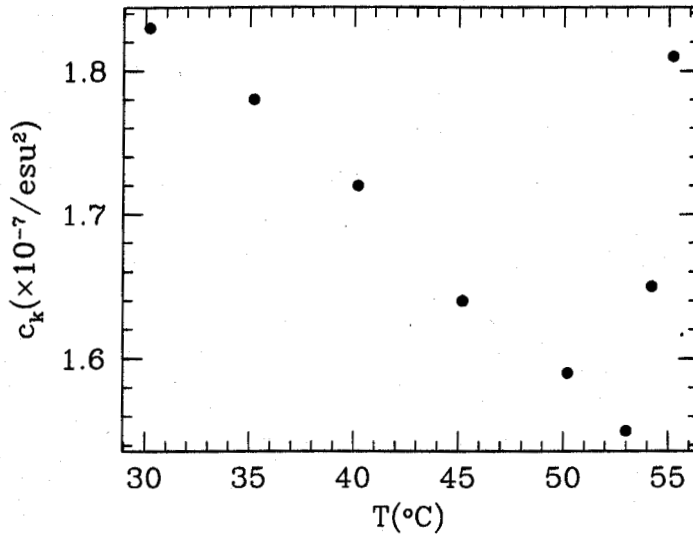


Figure 5.13: Variation of $c_k = \frac{\epsilon_0 \chi_k t}{12\pi}$ as a function of temperature.

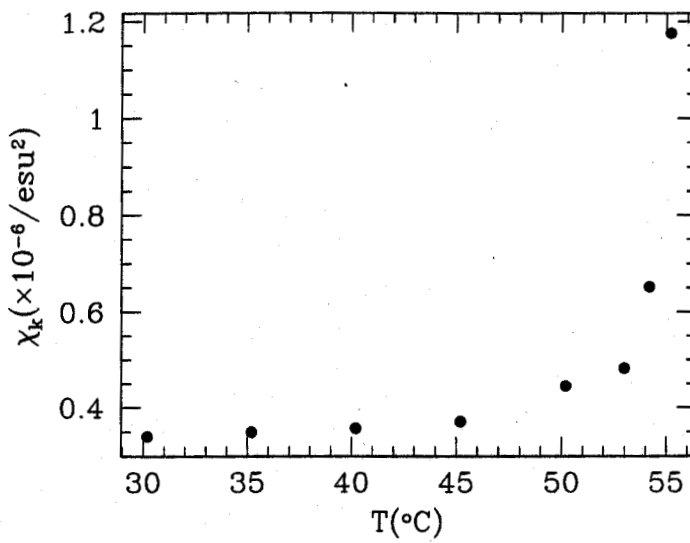


Figure 5.14: Variation of χ_k as a function of temperature.

Though $|c_{ql}|$ decreases with temperature, it is too small to account for the increase of c . By taking out the contribution due to c_{ql} we have calculated c_k (Figure 5.13) and hence the variation of the susceptibility χ_k (Figure 5.14) using Equation 5.32 with temperature using the known ϵ_a values [75]. χ_k has a rapid decrease as the temperature is lowered from T_{NI} , and it decreases rather slowly at lower temperatures. Thus the large increase in ϵ_a at lower temperature accounts for the unusual temperature dependence of c_{qk} .

5.4.4 Electrical Conductivity Measurements

The field and temperature dependences of the resistance of the sample are shown in Figure 5.15, from which we note the following features. (i) At low applied fields up to 187.5 esu the resistance decreases with increase of temperature in the nematic range, and has a positive jump of ~ 25 -30 % across the nematic-paranematic transition point, and decreases again at higher temperatures. (ii) In the lower temperature range (around 30°C), the resistance **increases** with field up to ~ 416.7 esu and then starts to decrease. (iii) The last observation is also related with an actual increase of resistance with temperature at higher fields in the lower temperature range. (iv) Beyond ~ 312.5 esu the resistance drops substantially as the nematic-paranematic transition temperature is approached. As the applied fields are now close to the critical value, this clearly indicates a critical enhancement of the electrical conductivity of the sample. (v) The last two effects which have opposite trends with temperature result in a broad peak in the resistance of the sample at higher fields (Figure 5.15). The peak shifts to higher temperatures at higher fields. (vi) Beyond the transition temperature, there is a very large increase in resistance in a narrow temperature range. The resistance shows a relatively sharp maximum and decreases at higher temperatures.

The anisotropic electrical conductivity in the nematic phase of the highly polar compound used in our experiment has two contributions: (i) The medium has unknown species of ionic impurities which contribute to the DC as well as AC conductivity of the sample. (ii) The dielectric constant $\epsilon_{||}$ relaxes at relatively low frequencies (ω , $\sim \text{MHz}$) in the nematic phase because of the nematic potential which generates an additional barrier for reorientation of the dipoles about the short axes of the molecules. As discussed by Schadt [78], the relaxation process increases the effective conductivity $\sigma_{||}$ of the medium. The excess conductivity increases as ω_r is approached. The strong heating effect due to this excess conductivity near ω_r has been experimentally studied by Schadt [33, 34]. However, this contribution normally **decreases** at higher temperatures as the order parameter, and hence the nematic potential as well as the friction coefficient for rotational motion decrease with increase of temperature, resulting in an increase in ω .

The ionic contribution to the conductivity is anisotropic as the mobility of the charges is higher along the director compared to its value in an orthogonal direction. The nematic is a weak electrolyte because of the impurity ions. Thus, electrolytic processes become relevant in the conduction mechanism [29]. In our experiment, the minimum field applied to the sample is 20.8 esu and if the dissociation constant producing ions in the medium is sufficiently small, we can expect that the bulk of the ions flow towards the electrodes under the action of the field to give rise to an initial surge after the field is reversed. It also leads to a depletion of charges in the bulk and hence to a reduced conductivity. In turn, there is a saturation of current at higher fields [79]. As the field is increased the effective average resistance of the sample **increases** as is indeed seen at low temperatures between 20.8 to 416.7 esu. Another concurrent effect of the field is the increase in the orientational order parameter, which in the compound used is quite considerable even at low temperatures, as discussed in Section 5.2.2. An increased order parameter would

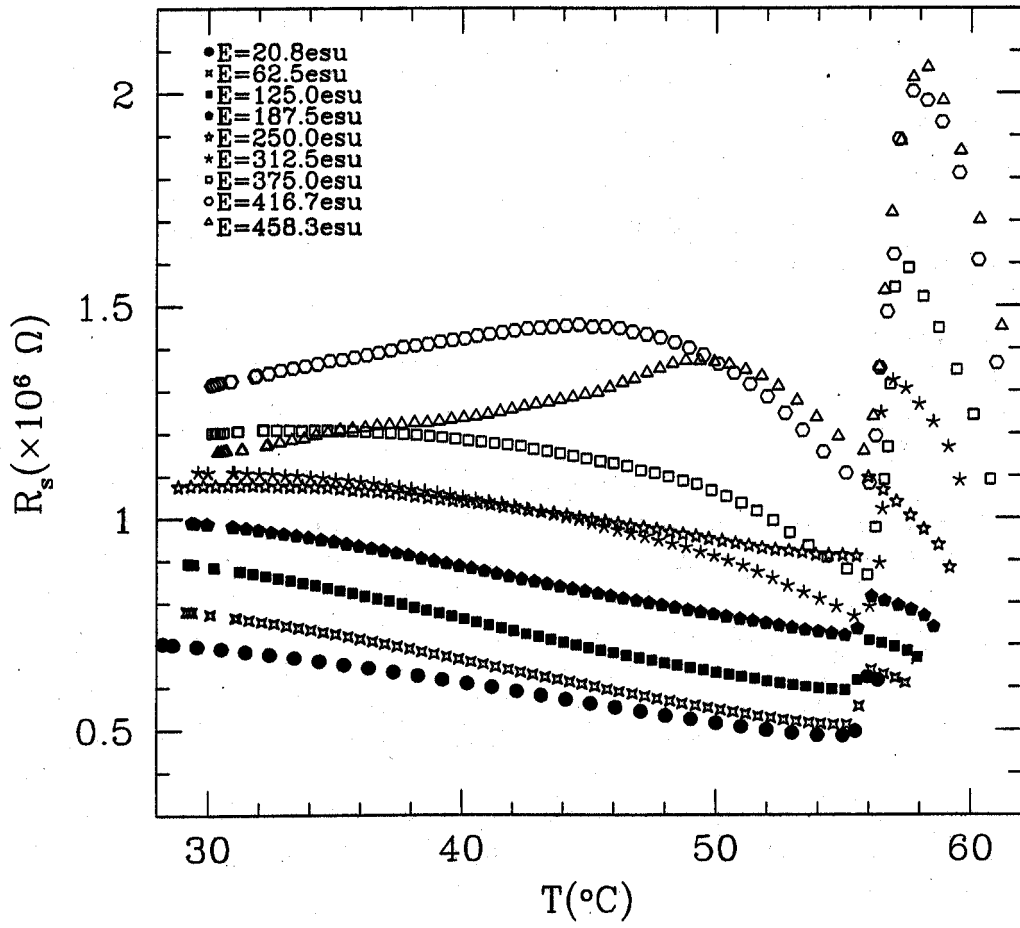


Figure 5.15: Temperature variations of the resistance of a $16 \mu\text{m}$ thick sample of CP7B at various values of the applied electric fields, $f=4111 \text{ Hz}$.

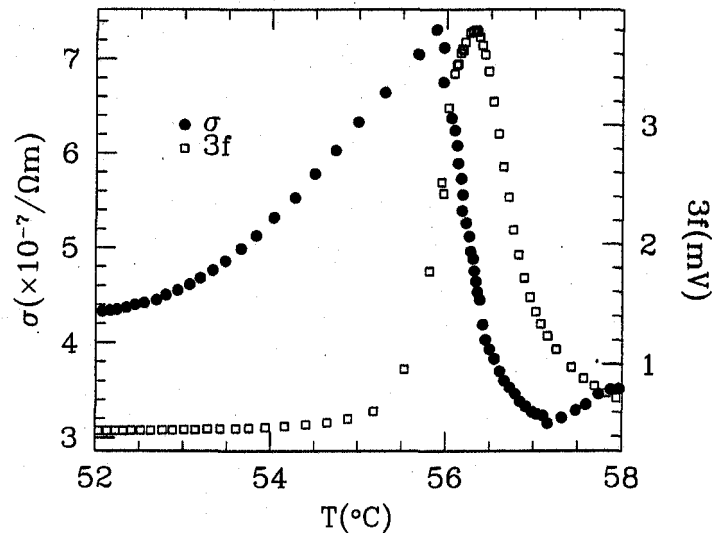


Figure 5.16: Temperature variations of the electrical conductivity and third harmonic signal of CP7B of a $12 \mu\text{m}$ thick sample under a field of 170V , $f=4111 \text{ Hz}$ (near the paranematic-nematic critical point).

imply an increased conductivity both due to the greater mobility of ionic impurities along A , the director, and due to a lowering of the dielectric relaxation frequency. This effect due to the field is opposite to the charge depletion effect discussed above. Apparently at $\sim 30^\circ\text{C}$ beyond 416.7 esu the former effect overtakes the latter and at higher fields the resistance *decreases* with field (Figure 5.15). Further, at low fields the temperature coefficient of resistance is negative, as the mobility of ions increases with temperature. As the field is increased to $\sim 250 \text{ esu}$, the resistance of the cell is practically independent of temperature at $\sim 30^\circ\text{C}$ due to the compensation of the pure temperature effect by that due to the decrease in orientational order at higher temperatures. Indeed above 375 esu the temperature coefficient of resistance has a *positive* sign at 30°C .

The most important effect on conductivity arises close to the nematic-paranematic transition point when the applied field is above 312.5 esu . We clearly see a sharp dip in R_s as this transition point is approached and a subsequent rise in R_s which is even sharper. As usual, the resistance starts decreasing with temperature after attaining a maximum. The dip in resistance is obviously connected with the field-induced critical point in the sample. We have made detailed measurements on the resistance of a $12 \mu\text{m}$ thick sample close to the critical point at 170 V ($E = 472 \text{ esu}$) which corresponds to a field which is close to the critical value. The conductivity of the sample is shown in Figure 5.16 on an enlarged temperature scale. We have also shown in the figure the temperature variation of the third harmonic signal which was also simultaneously measured. As we discussed in Section 5.2.1, the third harmonic signal is a direct measure of the susceptibility of the system. It exhibits an enhancement by *an* order of magnitude as the temperature is varied across the critical region. The third harmonic signal shows a nearly symmetric and narrow peak. The conductivity shows a peak at a temperature which is $\sim 0.4^\circ\text{C}$ *below* that corresponding to the third harmonic signal. Moreover, the conductivity shows a broader maximum, with a characteristic asymmetry with temperature.

Electrical resistance has been measured in other liquids exhibiting critical phenomena. Both in a binary mixture of two metals *viz.* bismuth and gallium as well as in an aqueous solution of isobutyric acid, the resistance has been shown to dip by a small fraction as the liquid-liquid critical temperature is approached from above [80, 81]. In these cases, dR/dT exhibits a critical divergence in these systems as T_c is approached. In our system, the enhancement in conductivity is indeed much larger, and as mentioned earlier, occurs at a temperature below T_c . We believe that the enhancement is **not** connected with ionic conductivity. It is probably caused by the critical slowing down of fluctuations as T_c is approached. As we have discussed in Section 5.4.1, the compound used *viz.* CP7B, in this experiment appears to have a fraction of the molecules in the *parallel* configuration. We can expect that unlike molecules with **antiparallel** configuration which form **pairs** due to a frustration effect, the parallel molecules will form relatively larger **polarised** domains [59]. The orientation polarisation of such domains begins to have a collective response as T_c is approached. We describe the enhancement of the conductivity in the framework of the Landau-Khalatnikov theory for critical slowing down.

When a system is close to a critical point, anomalies occur in a wide variety of dynamical properties such as viscosity coefficients and light scattering. Near this region both time and length scales diverge. Suppose a system is slightly away from the equilibrium state. Then the rate of approach of the order parameter S to equilibrium value S_{eq} is determined by the Landau-Khalatnikov transport equation [82]

$$\frac{dS}{dt} = \Gamma \frac{\partial F}{\partial S} \quad (5.35)$$

where Γ is a transport coefficient which does not possess any singularity in the vicinity of T_c and F is the free energy density. For the paranematic-nematic phase transition the free energy density is of the form (see Equation 3.12)

$$F(p, T, S) = F_o(p, T) - hS + \frac{A}{2}S^2 - \frac{1}{3}BS^3 + \frac{1}{4}CS^4 \quad (5.36)$$

where $h = \frac{1}{12\pi} \Delta\epsilon_o E^2 = -\mu_e E^2$. Expanding $\partial F/\partial S$ in a series of the difference $S - S_c$ (around the critical point) and expressing S_c and T^* in terms of T_c and the Landau parameters near the critical point we find that

$$\begin{aligned} \frac{dS}{dt} &= \Gamma a(T_c - T)(S - S_c) \\ &= \frac{1}{\tau}(S - S_c). \end{aligned} \quad (5.37)$$

Hence, it follows that τ is a relaxation time, which characterises the establishment of equilibrium in the vicinity of a critical point and is of the form

$$\tau = \frac{1}{a\Gamma(T_c - T)}. \quad (5.38)$$

Near the critical point we can expect that the critical slowing down will enhance the effective conductivity due to the dielectric relaxation which occurs at lower and lower frequencies. Equation 5.38 predicts the critical slowing down of the collective response as one approaches T_c . The dielectric relaxation will give rise to an effective conductivity [78]

$$\sigma_{\parallel}(\omega) = \frac{\epsilon_o(\delta\epsilon_{\parallel})}{1 + \omega^2\tau^2} \tau\omega^2 \quad (5.39)$$

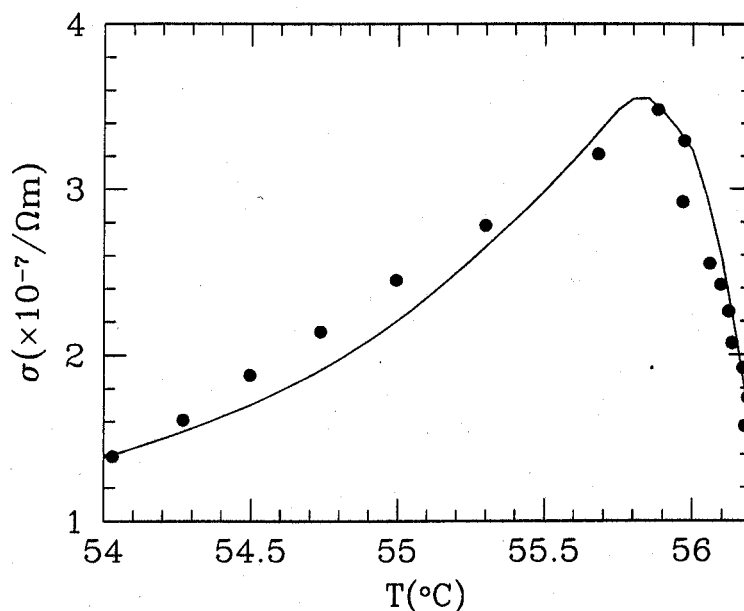


Figure 5.17: The fluctuation dependent part of the conductivity (points) compared with the theoretical variation (curve) assuming Landau-Khalatnikov slowing down of polarised domains. Points show the experimental data calculated from that shown in Figure 5.16.

where ϵ_0 is the vacuum dielectric constant and $\delta\epsilon_{\parallel}$ is the difference between the low frequency and high frequency dielectric constants. It can be seen from Equation 5.39 that a **peak** in conductivity occurs at $\omega\tau = 1$. We have used $f = \omega/2\pi$ of 4111 Hz in our experiments, and we can calculate the constant $a\Gamma$ in Equation 5.38 from the experimental data. Using Equations 5.38 and 5.39 we can then calculate σ_{\parallel} as a function of temperature at the measuring frequency. We compare this with the measured excess conductivity due to the critical slowing down, which is obtained by subtracting a linearly interpolated 'background' value from the measured value of σ_{\parallel} . The calculated value agrees with the measured excess at the peak position if we assume $\delta\epsilon_{\parallel} \simeq 3$. This is much smaller than $\epsilon_{\parallel} - n^2 \simeq 20$ (where n is the refractive index) which would be the value if the entire medium contributed to the relaxation mechanism. The small value of $\delta\epsilon_{\parallel}$ indicates that only a relatively small fraction of the molecules form the polarised domains which exhibit this collective response. Indeed with this assumption, the temperature variation of the excess conductivity is reasonably well reproduced (Figure 5.17).

As a result of this excess conductivity the sample heats up around this temperature much more than at temperatures far away from that corresponding to the peak in σ_{\parallel} . Consequently there is a scarcity of data points around this temperature. It is interesting to note that in other compounds like **octyloxycyanobiphenyl**, the conductivity shows a smaller enhancement as T_c is approached. Indeed in this case, the parallel configuration appears to be practically absent near T_c .

The above interpretation is supported by the fact that we have seen a small but clear peak in the **second harmonic** signal near T_c (Figure 5.18). As mentioned in Section 5.2.1 such a signal

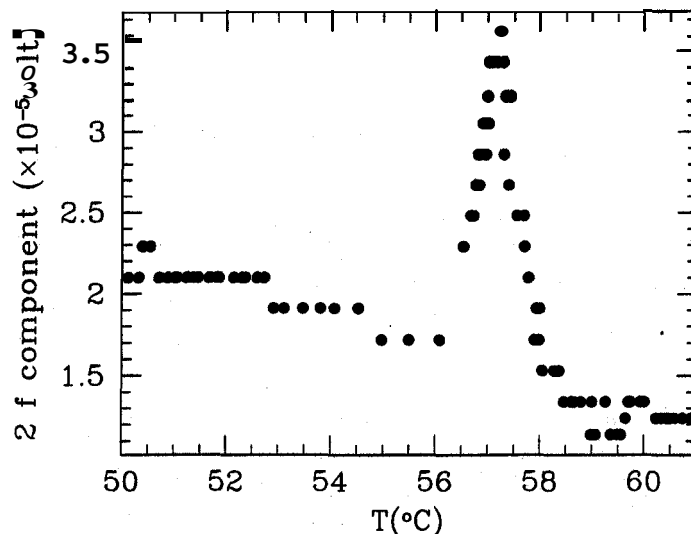


Figure 5.18: Divergence of the second harmonic signal in a $10\mu\text{m}$ thick sample of CP7B under 180 V, $f=4111$ Hz.

implies that the medium has polarised domains which are unable to reorient at the frequency of the applied voltage. Also, a second harmonic peak has not been seen in other compounds like, for example pentyl cyanobiphenyl.

5.4.5 Divergence of the Third Harmonic Component of the Electrical Signal

In Section 5.2.1 it has been shown that the third harmonic component (V_3) of the electric signal is a measure of the order parameter susceptibility. Figures 5.19 and 5.20 show the variations of the amplitude and phase of the third harmonic component of electrical signal as a function of temperature for $V=170$ V and an frequency of 4111 Hz. As described in the previous section near the critical region the amplitude of the third harmonic component which is a measure of χ_E diverges. The phase shows a broad peak around the critical region in the center of which there is a small dip.

The extraction of a critical index from the data on the third harmonic signal is somewhat delicate. As the conductivity also is quite nonlinear around the critical point, the contribution from σ_{\parallel} to the response has to be accounted for. Here we do not undertake this analysis. The observed divergence (Figure 5.19) serves to show that we have indeed reached the critical region.

5.4.6 Field Induced Nematic-Nematic Phase Transition (?)

In two independent experiments we noticed that the intensity of light scattered by twist fluctuations in the medium showed a sharp increase at $\sim 33^\circ\text{C}$ when the sample was cooled under a field of ~ 600 esu (Figure 5.21). This clearly indicates that a phase transition occurs under these conditions. We did not notice this enhancement when the field was significantly smaller than the value given above. Also ϵ_{\parallel} increases by a small amount around this temperature (Figure 5.22) and the resistance shows a small positive jump (Figure 5.23). Conoscopic observations on

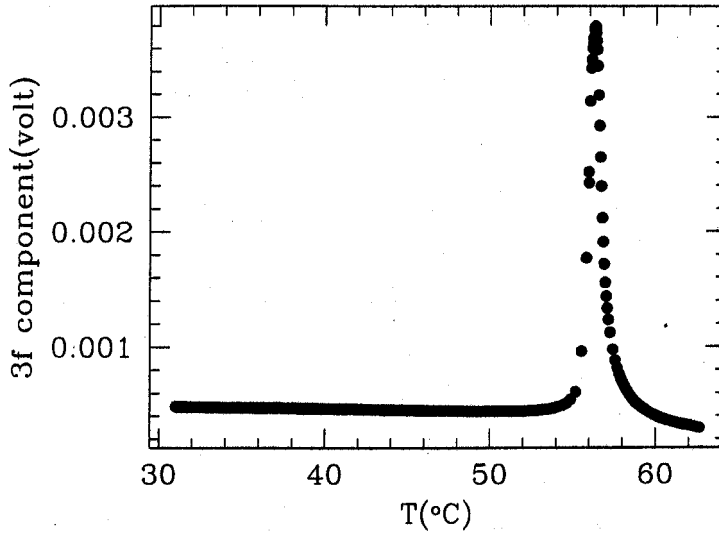


Figure 5.19: Variation of the third harmonic component of the electrical signal as a function of temperature over the nematic range $V=170$ V, $f=4111$ Hz $d = 12\mu\text{m}$.

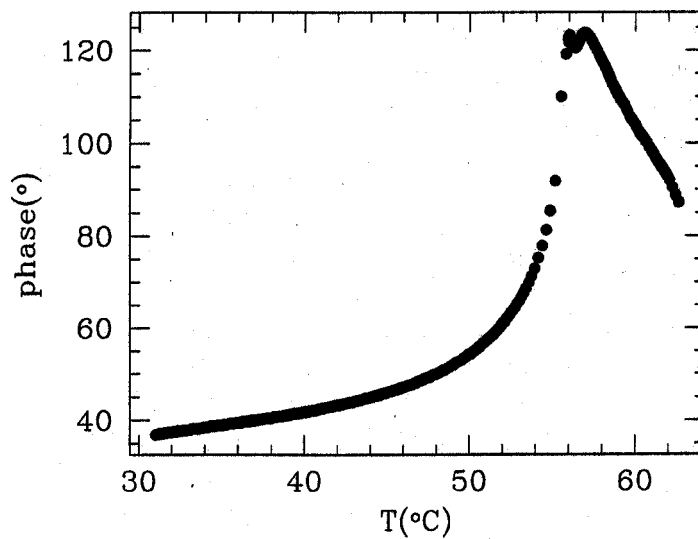


Figure 5.20: Variation of the phase of the third harmonic component of the electrical signal as a function of temperature in the entire nematic range of CP7B. $d=12\mu\text{m}$ $V=170$ V, $f=4111$ Hz.

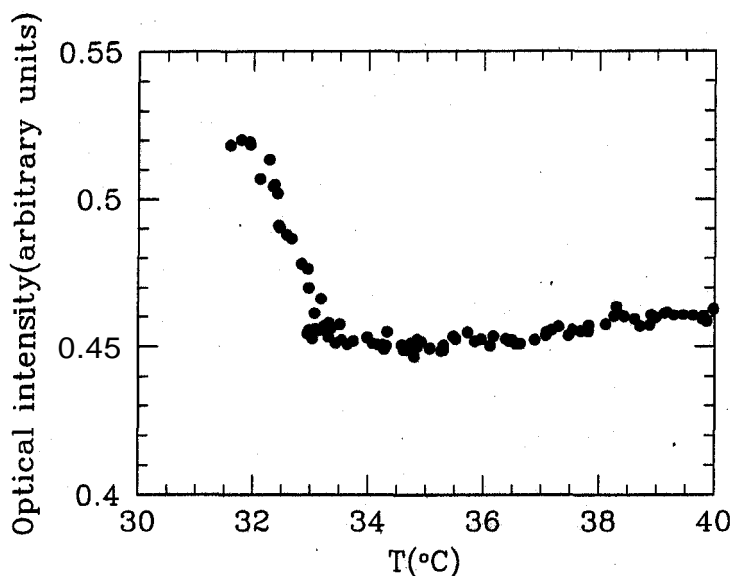


Figure 5.21: Temperature variation of the light scattered from twist fluctuations in a $10\mu\text{m}$ thick sample of **CP7B** subjected to 180 V, $f=4111$ Hz. Note the large enhancement at 33°C .

thick enough samples ($\sim 40\mu\text{m}$) under a similar field indicated that the medium continues to be uniaxial below this temperature. We subjected a *homogeneously* aligned sample to a transverse field of a similar magnitude in a gap ($\sim 12\mu\text{m}$ wide) etched in an ITO coated plate, and did not find any evidence for a transition to the smectic A phase by direct texture observations. As we discussed in Chapter 4 the molecular theory in which the polar molecules can have antiparallel and parallel mutual configurations, predicts that the concentration of the latter increases as the temperature is lowered. In **CP7B** this leads to an excess ϵ_{\parallel} at lower temperatures. Further the possibility of a jump in the concentration of parallel configuration and hence a nematic-nematic transition line, such that the long range order has the same nature in the two phases has also been predicted [59]. This transition is rather weak and hence hard to detect and can exhibit a critical point under the action of the field.

Indeed we think that the large increase in the scattered intensity implies a weak transition of this kind. If this is the case it once again confirms that the compound used in the present experiments has a fraction of the molecules in the parallel configuration, the remaining ones having the antiparallel short range order. Indeed using specific heat measurements a nematic-nematic transition has been reported earlier in a binary mixture of strongly polar compounds [83] which has been seen as a continuation of a smectic A_1 - A_d transition line. In **CP7B** that we have studied, there is no smectic phase and the possibility of an N_1 - N_d transition would be due to a change in the short range order even in the absence of a smectic phase in the vicinity of the transition. However, more detailed experiments are required to confirm that the transition is between two nematic phases.

The results in this chapter are consistent with the trends expected on the basis of the molecular model described in the previous chapter in which the highly polar compounds prefer to have antiparallel pairs at higher temperatures and parallel configurations at lower temperatures. We may mention here that from dielectric measurements on dilute solutions of a lower homologue of **CP7B**, viz., **CP4B**, Dunmur [84] found evidence for parallel correlations between the polar molecules when the concentration was **quite** low. As the concentration was increased the an-

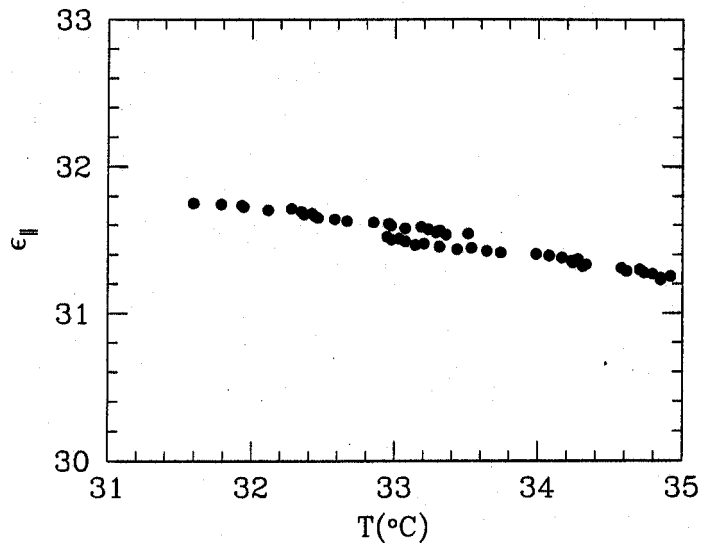


Figure 5.22: Temperature variation of $\epsilon_{||}$ $10\mu\text{m}$ thick sample of CP7B subjected to 180 V $f=4111$ Hz. Note the small jump around 33°C .

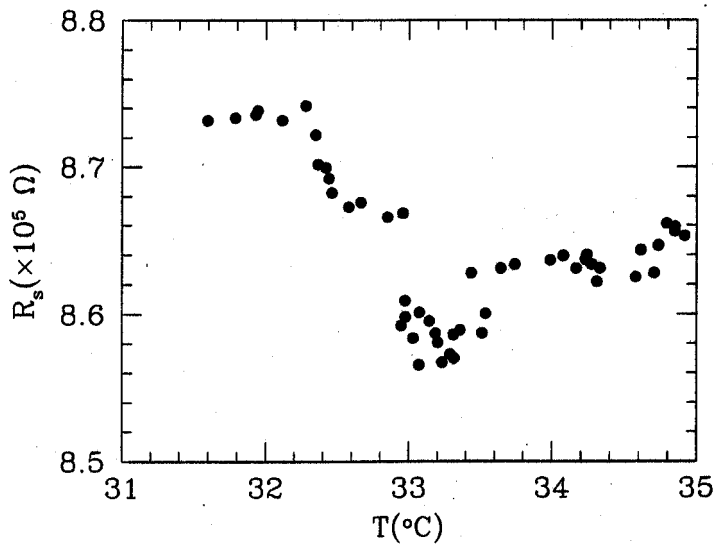


Figure 5.23: Temperature variation of R_s in a $10\mu\text{m}$ thick sample of CP7B subjected to 180 V, $f=4111$ Hz. Note the jump at 33°C .

tiparallel correlation was favoured. On the other hand our results on the pure compound show that parallel correlations are favoured especially at lower temperatures, or higher densities, as predicted by our molecular model. We interpret the conductivity peak near T_c as arising from a critical slowing down of macroscopic polarised domains of molecules which have the parallel orientation. Indeed the detection of a significant second harmonic peak at T_c which implies the presence of polarised domains that do not reorient with the field, appears to support this idea.

Finally, we have found evidence for a field induced transition deep inside the nematic range. As the lower temperature phase is neither **biaxial** in nature nor exhibits the textures of smectic A, we interpret this to be a nematic-nematic phase transition in which the fraction of molecules with the antiparallel orientation increase **as** the temperature is raised across the transition. We may also note that there is a considerable body of theoretical work on the possibility of a **polar** nematic phase when the molecules carry a large dipole moment (see for example [85]). To our knowledge such a phase has not yet been discovered. Our observation of a strong **polar short range order** may indicate one possible route to the realisation of a polar nematic liquid crystal.